ACS APPLIED MATERIALS & INTERFACES

Research Article

www.acsami.org

Self-Organization of Ions at the Interface between Graphene and Ionic Liquid DEME-TFSI

Guangliang Hu,[†,‡,§] Gaind P. Pandey,[∥] Qingfeng Liu,[§] Radhika S. Anaredy,[⊥] Chunrui Ma,[*,†] Ming Liu,[‡] Jun Li,[∥] Scott K. Shaw,[⊥] and Judy Wu[*,§]

[†]State Key Laboratory for Mechanical Behavior of Materials, Xi'an Jiaotong University, Xi'an, Shaanxi 710049, China

[‡]School of Microelectronics, Xi'an Jiaotong University, Xi'an, Shaanxi 710049, China

[§]Department of Physics and Astronomy, University of Kansas, Lawrence, Kansas 66045, United States

[∥]Department of Chemistry, Kansas State University, Manhattan, Kansas 66506, United States

[⊥]Department of Chemistry, University of Iowa, Iowa City, Iowa 52242, United States

Supporting Information

ABSTRACT: Electrochemical effects manifest as nonlinear responses to an applied electric field in electrochemical devices, and are linked intimately to the molecular orientation of ions in the electric double layer (EDL). Herein, we probe the origin of the electrochemical effect using a double-gate graphene field effect transistor (GFET) of ionic liquid *N*,*N*-diethyl-*N*-(2-methoxyethyl)-*N*-methylammonium bis(trifluoromethylsulfonyl)imide (DEME-TFSI) top-gate, paired with a ferroelectric $Pb_{0.92}La_{0.08}Zr_{0.52}Ti_{0.48}O_3$ (PLZT) back-gate of compatible gating efficiency. The orientation of the interfacial molecular ions can be extracted by measuring the GFET Dirac point shift, and their dynamic response to ultraviolet−visible light and a gate electric field was quantified. We have observed that the strong electrochemical effect is due to the TFSI anions self-organizing on a treated GFET surface. Moreover, a reversible order−disorder transition of TFSI anions self-organized on the GFET surface can be triggered by illuminating the interface with ultraviolet−visible light, revealing that it is a useful method to control the surface ion configuration and the overall performance of the device.

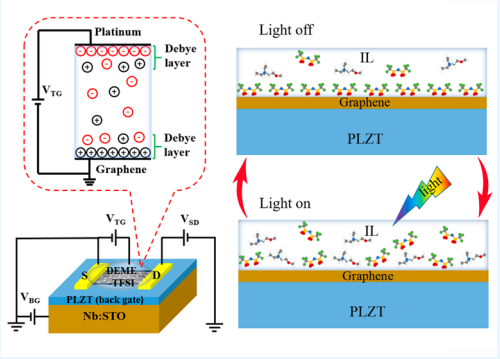

KEYWORDS: *self-organization, graphene field effect transistor, ionic liquid, interface, electrochemical effect*

INTRODUCTION

Graphene and carbon nanostructures have been widely used as electrodes for electrochemical devices, in which the graphene/electrolyte interface is a critical component affecting the device performance.[1−6] In these devices, an electric double layer (EDL) with Debye thicknesses typically on the order 1−2 nm forms at the graphene/electrolyte interface.[7,8] Since the applied electric field through the electrolyte is primarily attenuated across the EDL, the distribution and alignment of ions in EDL have a profound effect on the performance of the electrochemical devices. This is particularly true with the large, polarizable, and often asymmetric ions found within (ILs) which create stark differences when compared to their aqueous or organic counterparts.[9] Some of these differences have engendered new theories and experimental interpretations which remain under scrutiny. Multiple reports in the literature show that ILs create unprecedented ordering near surfaces that may extend into the bulk.[10−14] The ensemble dynamics of ionic liquids have been reported to be several orders of magnitude slower than those for molecular liquids.[15,16] These effects near electrodes are particularly relevant here, but similarly difficult to characterize within conventional, dilute electrolyte models.[17] Understanding the interfacial behavior of the molecular ions in ILs is therefore important to the fundamental science of graphene-based nanohybrids and to the applications of graphene. However, it is generally difficult to separate the behavior of the interfacial electrolytes from that of their bulk counterparts.[4,18,19]

Graphene field effect transistors (GFETs) display channel conductance that is sensitive to interface electrical charges with high bipolar electrical susceptibility. This provides a unique, interfacial charge probe.[20] In our recent work, a GFET was inserted between a ferroelectric $Pb_{0.92}La_{0.08}Zr_{0.52}Ti_{0.48}O_3$ (PLZT) back-gate and an ionic liquid *N*,*N*-diethyl-*N*-(2-methoxyethyl)-*N*-methylammonium bis-(trifluoromethylsulfonyl)imide (DEME-TFSI) top-gate for probing the interface dipole−dipole interactions in response to dc and pulsed gate voltages.[21] This double-gate GFET configuration has a unique advantage in high-efficiency gating from both gates. PLZT has high specific capacitance of ∼2.1 μF cm^{-2} due to the large permittivity $\varepsilon_r \sim 1200$[22,23] that is much higher than that of normal dielectric gate materials ($\varepsilon_r < 10$; see

Received: July 24, 2017
Accepted: September 18, 2017
Published: September 18, 2017

DOI: 10.1021/acsami.7b10912
ACS Appl. Mater. Interfaces 2017, 9, 35437−35443

details in the Supporting Information). DEME-TFSI has a comparable specific capacitance (~1.7 μF cm^{-2} at 1 Hz by ac measurement, see Figure S1). These unique properties allow observation of the GFET's Dirac point from both the top- and back-gates within a similar gate voltage range of ±1.0 V, well below the electrical breakdown voltage of the IL.[22,24,25] In the double-gate DEME-TFSI/GFET/PLZT devices, we have found that, in a large range of the gate field, the combined effect of the two gates is electrostatic, which means that the graphene Dirac point shifts linearly with the total field as a superposition of electric fields from the two gates. However, a highly nonlinear behavior was observed when the ionic liquid (IL) top-gate voltage fell in a certain range, which seems to correlate intimately with residual charges due to molecular ions at the interface. This so-called electrochemical effect also has been observed on other carbon-based electrodes used for electrochemical devices with a detrimental effect on the performance of the devices.[26−28] Nevertheless, the microscopic mechanism of the electrochemical effect is barely understood, which motivated some recent investigations.[11,29−32] Parr et al. observed an electrode (gold)/electrolyte "thermodynamic" interfacial structure (at 0.0 V) containing an approximately complete layer of anions and speculated that this may be due to the coordination chemistry of the TFSI anion on gold.[32] On the other hand, Xu et al. proposed that some functional group of the interfacial molecular ions may prefer to orient under an external electric field.[31] In order to achieve a thorough understanding of the electrochemical effect, we investigate the dynamic behavior of the interface molecular ions on double-gate DEME-TFSI/GFET/PLZT devices in response to ultraviolet−visible light in the spectrum 200−1000 nm. Our data shows that self-organized TFSI anions are formed on graphene and are sensitive to the surface conditions of the graphene. Consequently, a strong electrochemical effect occurs. Remarkably, a reversible order-to-disorder transition of the TFSI anions was also found in response to ultraviolet−visible light illumination.

MATERIALS AND METHODS

Fabrication of Epitaxial PLZT Film. A KrF excimer pulsed laser deposition system with a wavelength 248 nm has been used to grow the epitaxial PLZT thin films with a thickness of 500 nm on (001) Nb-doped $SrTiO_3$ (Nb:STO) single-crystalline substrates. The growth condition was selected under an oxygen pressure of 150 mTorr at 680 °C. The laser energy density was about 2.0 J cm^{-2} with laser repetition rate of 5 Hz. After the growth, the PLZT thin films annealed at the growth temperature for 15 min in pure oxygen (350 Torr) and then naturally cooled down to room temperature.

Graphene Fabrication and Transfer. Single-layer graphene of typically 1 × 1 cm^2 in dimension was grown at ~1000 °C in CH_4/H_2 (4:1) gas mixture in a chemical vapor deposition system on commercial polycrystalline copper foils (Sigma-Aldrich) of 25 μm in thickness.[33,34] Graphene was then transferred onto the PLZT films using a similar procedure reported in our previous work.[21,24] Briefly, poly methyl methacrylate (PMMA) was spin-coated on a graphene/Cu sheet. The sample was then immersed into copper etchant (CE100) to remove the copper foil. After the copper foil is fully dissolved, the PMMA/graphene was rinsed with deionized (DI) water multiple times before being transferred onto PLZT thin film. After the transfer, the PMMA/graphene/PLZT assembly was baked in air at 150 °C for 1 h to eliminate moisture. Finally, the PMMA on the graphene was removed with acetone, and then rinsed by isopropyl alcohol to remove residues on the surface of the graphene. Vacuum cleaning was applied to most samples for further removal of the residues.[25,35]

Double-Gate GFET Fabrication. A two-step photolithography process was applied for the GFET fabrication, and the details of the process have been reported previously.[21] In the first photolithography, the source and drain electrodes were defined on graphene, which was followed with electron beam evaporation of 2 nm titanium/88 nm gold electrodes and liftoff. The second photolithography was applied to define the GFET channel, and the rest of graphene was removed by using oxygen plasma in a reactive ion etcher (RIE, Torr International). The RIE time was 150 s under 6.7 mTorr oxygen partial pressure at 20 W RF power. The graphene channel was 20 (width) × 10 (length) μm^2. Ionic liquid DEME-TFSI was cast on the GFET channel as the top-gate, and the top-gate electric field was applied using a platinum wire (50 μm in diameter) immersed in the IL. DEME-TFSI was chosen since it has a large electrochemical window of ±3 V and comparable gating efficiency to that of PLZT.[34] This compatibility is critical in operating the double-gate GFETs to avoid the gate leakage. In addition, DEME-TFSI is transparent to visible light[24] to allow perturbation of the EDL using visible illumination.

Double-Gate GFET Characterization. The transport properties of the double-gate GFETs were characterized using an Agilent B1500A semiconductor device analyzer in a high-vacuum probe station of <2 × 10^{-6} Torr at room temperature. A broad-band light source (JUNGONG) was used for manipulation of the interface molecular ions. The power intensity was calibrated using a Coherent FieldMaxII power meter with OP-2 probe.

RESULTS AND DISCUSSION

The schematic of DEME-TFSI/GFET/PLZT double-gate GFET is shown in Figure 1a. Two EDLs are illustrated

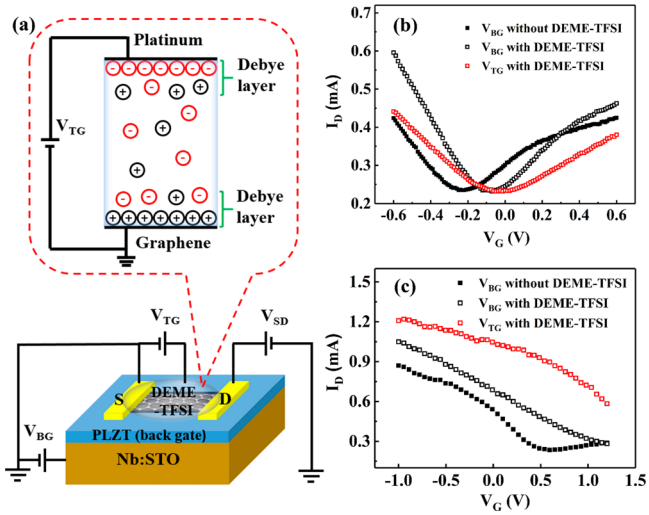

Figure 1. (a) Schematic of the DEME-TFSI/GFET/PLZT double-gate GFET and cartoon of the electrical double layers formed at the interface between DEME-TFSI and the platinum top-gate electrode, and between DEME-TFSI and graphene. (b) I_D−V_G curves of the GFET without (solid black) and with (open black and red) DEME-TFSI, and (c) the same GFET after the DEME-TFSI had been removed (solid black) and reintroduced (open black and red).

respectively at the interfaces of DEME-TFSI/Pt and DEME-TFSI/GFET (inset of Figure 1a). Please note that the applied total top-gate voltage $V_{TG} = V_{TG,GFET} + V_{TG,Pt}$ is split between the two interfaces of DEME-TFSI/Pt and DEME-TFSI/graphene. Considering that the DEME-TFSI/Pt has a much larger interface area than the DEME-TFSI/graphene, the $V_{TG,Pt}$ only takes a small proportion (<~15%) of the V_{TG} (as detailed in the Supporting Information). The source-drain current I_D was measured at the varied gate voltage V_G on GFET (of either top- or back-gate) using an Agilent B1500A semiconductor

DOI: 10.1021/acsami.7b10912
ACS Appl. Mater. Interfaces 2017, 9, 35437−35443

device analyzer in a probe station with a base pressure of 5 × 10^{-6} Torr. Figure 1b shows the I_D−V_G curves of a GFET/PLZT device with a pristine graphene channel surface before and after the application of the DEME-TFSI top-gate. A characteristic feature is in the shift of the Dirac point (V_{Dirac}) closer to zero voltage after the application of the top-gate, using either back-gate (V_{BG}, open black) or top-gate (V_{TG}, open red) voltage sweep. The gating efficiency of the IL top-gate is slightly lower than that of the PLZT back-gate, which is due to the fact that its effective specific capacitance (~1.4 μF cm^{-2} at 1 Hz) is smaller than that of the PLZT back-gate (~2.1 μF cm^{-2} at 1 Hz) as detailed in the Supporting Information. It should be mentioned that this shift has been observed on multiple samples irrespective of the original polarity of the V_{Dirac} shift.[21] This shift may be explained by the molecular ions in the EDL having the opposite polarity to compensate the residual interfacial charge on the GFET/PLZT devices with a pristine graphene surface.

Figure 1c depicts the three I_D−V_G curves measured on the same device after the device went through multiple exposures of DEME-TFSI and isopropanol for rinsing off the DEME-TFSI. Several major differences can be clearly observed. First, the V_{Dirac} of the device before the reapplication of the top-gate (solid black) shifted positively to ~0.58 V and is much larger than when the graphene surface was pristine (−0.22 V, Figure 1b, solid black), which means that a substantial amount of negative charges were accumulated on the graphene surface due to the chemical exposures, causing a significant hole-doping in the GFET channel. Second, in both V_{BG} (open black) and V_{TG} (open red) traces of Figure 1c, the V_{Dirac} further shifted to larger positive voltages beyond the measurement range, instead of shifting toward zero as in the pristine case. The further positive shift of the V_{Dirac} after the top-gate reapplication indicates that additional negative charges accumulated on the interface of the DEME-TFSI/GFET after reapplication of the ionic liquid top-gate.

The presence of the excess negative charge strongly affects the gate tunability of the GFET transport properties. Figure 2a,b is the I_D−V_{BG} curves taken on the same GFET device under applied gate voltages with graphene surface conditions similar to Figure 1b,c, respectively. For the device with a pristine graphene channel surface (Figure 2a), the V_{Dirac} point shifts linearly with V_{TG}, and this trend is shown in Figure 2c (black squares). The slope of these I_D−V_{BG} curves at different V_{TG} biases for both electron and hole branches is nearly invariable (Figure 2c blue circles). Furthermore, the two I_D−V_{BG} curves in Figure 2a taken at V_{TG} = 0.0 V before (black) and after (pink) application of the negative V_{TG} biases almost coincide, indicating a reversible process. Specifically, the V_{Dirac} values of the two curves differ by only ~0.03 V, indicating negligible accumulation of charged ions on the DEME-TFSI/GFET interface when the V_{TG} was removed. These observations indicate that electrostatic effects dominate in the double-gate GFETs with a pristine GFET channel surface. However, the electrostatic effect can be significantly reduced by rinsing the ionic liquid away, which necessarily exposes the graphene channel to organic solvent, i.e., isopropanol. As shown in Figure 2d (black squares), after rinsing the ionic liquid away with isopropanol, the V_{Dirac} (extracted from Figure 2b) shift with V_{TG} is highly nonlinear for V_{TG} < −0.8 V, and the shift of V_{Dirac} from V_{TG} = −1.0 to +1.0 V was estimated at more than 2.0 V, which is much greater than that expected from the electrostatic effect. Moreover, there is a large difference in I_D−V_{BG} curves measured at V_{TG} = 0.0 V before (black) and after (pink) the bias of V_{TG} = −1.0 V was applied (Figure 2b).

For the recording of possible chemical contamination on the graphene channel, Raman measurements (Figure 3a) are performed on the pristine graphene, graphene covered with DEME-TFSI, and graphene after washing DEME-TFSI by isopropanol. As shown in Figure 3a, the 2D band at 2695 cm^{-1} and the G band at ~1583 cm^{-1} with a ratio of the 2D band to the G band (I_{2D}/I_G) of over 1.5 are characteristic of monolayer graphene,[33] while the negligible D band (~1350 cm^{-1}) indicates that the graphene is largely defect-free throughout these treatments.[36] When DEME-TFSI was cast on graphene, a

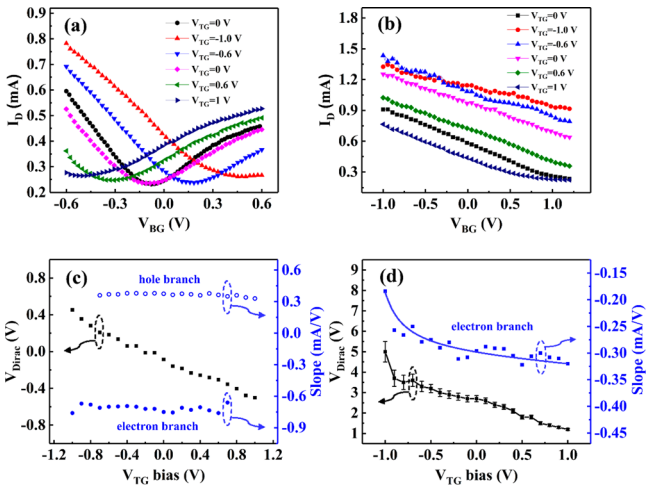

Figure 2. I_D−V_{BG} curves at different V_{TG} biases on the following: (a) a GFET with a pristine DEME-TFSI/graphene interface, and (b) the same device after rinsing off the ionic liquid with isopropanol and reintroducing the IL top-gate again. (c, d) V_{Dirac} and gating efficiencies at different V_{TG} biases measured from parts a and b, respectively.

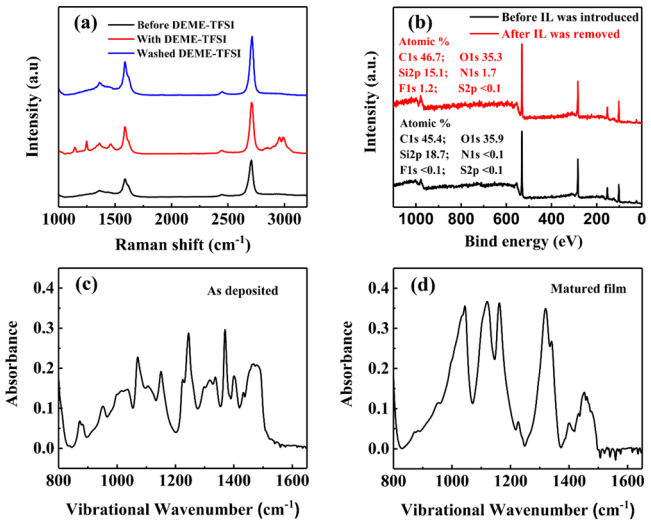

Figure 3. (a) Raman spectra of the GFET without and with DEME-TFSI, and after the DEME-TFSI was washed away by isopropanol. (b) XPS spectra of the GFET before DEME-TFSI was introduced (black), and after the DEME-TFSI was washed away by isopropanol (red). The infrared spectrum acquired from freshly deposited DEME-TFSI film (c), and that acquired from a film (d) that has been allowed to mature for 170 min.

DOI: 10.1021/acsami.7b10912
ACS Appl. Mater. Interfaces 2017, 9, 35437−35443

series of small peaks of ~1140, ~1247, ~1460, ~2955, and 2990 cm^{-1} appear in the Raman spectra (red).[37] After the DEME-TFSI was washed away by isopropanol, these small peaks disappear (green), demonstrating the existence of a trace of residual amount of DEME-TFSI absorbed on graphene surface is negligible. X-ray photoelectron spectroscopy (XPS) was further performed on the pristine graphene sample on a SiO_2(90 nm)/Si substrate before introduction of the DEME-TFSI and the same graphene sample after removal of the DEME-TFSI, as shown in Figure 3b. As it is expected, both XPS spectra exhibit a dominant C 1s peak at ~284.5 eV, verifying the formation of sp^2-hybridized carbon with most carbon atoms remaining embedded within the honeycomb lattice,[38] while the detected O and Si with a constant atomic ratio of ~2 follow the stoichiometry of bulk SiO_2 substrate. For the pristine graphene sample before introduction of the DEME-TFSI, no trace of any N or F impurities was detected on the pristine sample (Figure 3b, black). In stark contrast, a trace of N (1.7% atomic ratio) and F (1.2% atomic ratio) elements was detected on the same sample with removal of DEME-TFSI, confirming the existence of a trace of DEME-TFSI absorbed on the graphene surface (Figure 3b, red). These results reveal that a self-organized TFSI lattice probably forms at the DEME-TFSI/GFET interface, as reported in other electrolyte/electrode interfaces.[39,40] This is confirmed by the infrared reflection absorption spectra (IRRAS) of a DEME-TFSI film on a graphene-modified silver substrate. Figure 3c shows the IR profile as the IL film is being deposited, and Figure 3d is the same IL film 170 min after the film deposition is stopped, allowing maturation to take place. Comparison of the two IRRAS results reveals changes that are characteristic of long-range ordering as reported previously.[40] The peaks located at 1069, 1149, 1244, and 1366 cm^{-1} in Figure 3c correspond to SNS, SO_2-symmetric, CF_3, and SO_2-asymmetric stretches from the TFSI anion, respectively, indicating that the TFSI anion layer forms at the IL/graphene interface. The 170 min time frame for the reorientation process is somewhat longer than what might be predicted from earlier work on bare Ag surfaces. We attribute this to the graphene-modified substrate used here, which exposes a different set of intermolecular interactions between substrate and the IL film.

It is known that self-organization of molecules involves only low-energy van der Waals interactions between molecules and the interface; hence moderate-energy activation, such as ultraviolet−visible light illumination (emission spectrum shown in Figure S2), may perturb the molecular organization. For exclusion of other artificial effects that might affect the dynamic behavior of the ionic liquid, I_D-V_{BG} curves were first taken in completely dark conditions during a comparable time frame of 1−2 h, and the results are illustrated in Figure 4a. The black data set shows the I_D-V_{BG} curve of the device that has been exposed to DEME-TFSI and then cleaned with isopropanol (presumably leaving a "pinned" layer of TFSI adsorbed on the graphene). After reapplication of the DEME-TFSI top-gate, seven additional I_D-V_{BG} curves were acquired every 10 min for 1 h. Figure 4a shows that these curves are similar to those shown in Figure 2b, displaying only a slight positive shift in the potential of the Dirac points with time. To exclude influence of water or other airborne species, the probe station chamber was pumped down and maintained at ~1 Torr for about 12 h before backfilling to 720 Torr with clean N_2. It can be clearly seen from Figure 4b that the I_D-V_{BG} curves

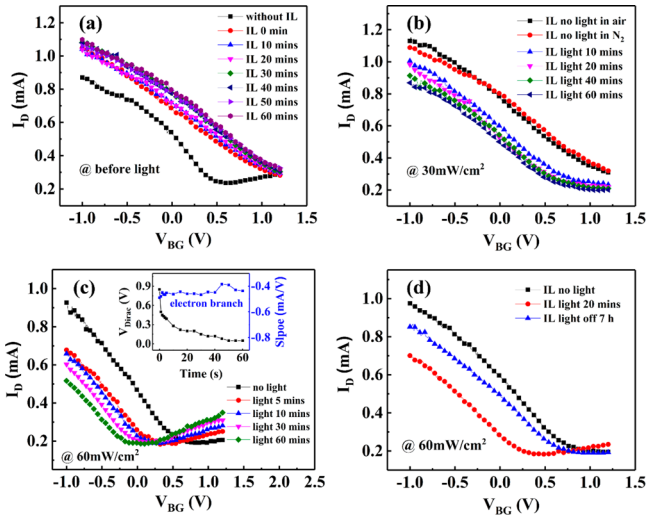

Figure 4. I_D-V_{BG} curves taken (a) in the dark after application of the DEME-TFSI top-gate for different times, (b) at different light exposure times at an intensity of 30 mW cm^{-2}, (c) at different light exposure times at an intensity of 60 mW cm^{-2} (inset: V_{Dirac} and gating efficiency as a function of the light exposure time), and (d) through a cycle of the light on and off (light intensity: 60 mW cm^{-2}).

measured in air (black) and in N_2 (red) overlap well, indicating no significant influence of water from air.

Then, the device was illuminated with different light-density ultraviolet−visible light. As shown in Figure 4b,c, it can be clearly seen that the I_D-V_{BG} curve shifts to more negative potentials with increasing illumination time, and the rate of the shift is linearly related to the light intensity (Figure S3). A light intensity of 30 mW cm^{-2} caused equilibrium after ~20 min illumination (saturated V_{Dirac} is ~1.0 V, Figure 4b), while higher light intensity of 60 mW cm^{-2} caused a larger shift (saturated V_{Dirac} is ~0.0 eV) after ~60 min (Figure 4c). These phenomena indicate that the light perturbation seems efficient to disrupt this weakly attached interfacial charged ion layer in the time frame of tens of minutes at a moderate light intensity, and the negative potential shift of V_{Dirac} implies that the TFSI anions attached to the GFET channel surface can be released via applying ultraviolet−visible light. Importantly, the observation of V_{Dirac} ~ 0.0 eV further confirms the hypothesis of an adsorbed TFSI anion layer at the IL/graphene interface. It is noted that from Figure 4d the I_D-V_{BG} curve measured after the light was switched off for 7 h (blue) almost coincides with the initial condition (black), indicating a reversible, spontaneous self-organization of the anion layer at the IL/graphene interface which is similar to other reports.[40] According to a relationship between the time required for interfacial ion reorientation and viscosity, DEME-TFSI would likely need several hours to complete an interfacial reorientation of ions.[40] This seems consistent with the time frame observed in this work from the completed I_D-V_{BG} curve's positive potential shift after the light is turned off, back to the original shape before light illumination (Figure 4d). The results obtained in this work shed light on the microscopic mechanism of the electrochemical effect observed on the DEME-TFSI/graphene interface (Figure 5a,b), which may be applied to a large number of electrolyte/electrode interfaces. First, the chemical nature of the interface plays a critical role in the formation of self-organized cation or anion molecular layers in the EDL, which results in a pronounced "electrochemical effect", and a highly nonlinear response to the

DOI: 10.1021/acsami.7b10912
ACS Appl. Mater. Interfaces 2017, 9, 35437−35443

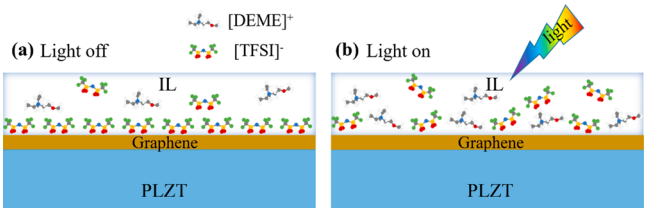

Figure 5. Schematic description of (a) interface-facilitated self-organization of the TFSI anions, and (b) light activation of the self-organized interfacial TFSI anion layer.

applied electric fields (Figure 5a). Second, visible light can weaken and even remove the adsorption of cation or anion molecule layers on the interface (Figure 5b).

Figure 6a shows a group of I_D-V_{BG} curves measured after exposure of white light of 60 mW cm^{-2} for 1 h, at different V_{TG}

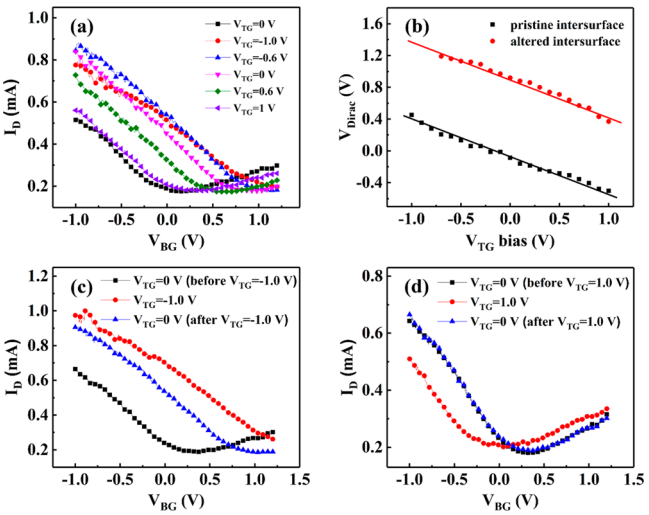

Figure 6. (a) I_D-V_{BG} curves at different V_{TG} biases immediately after the 1 h of light illumination of 60 mW cm^{-2}. (b) $V_{Dirac}-V_{TG}$ curves of a GFET, with pristine interface (black) and modified interface but after 60 mW cm^{-2} white light illumination (red). I_D-V_{BG} curves after light treatment going through opposite V_{TG} bias sequences starting from (c) −1.0 V and (d) + 1.0 V.

biases, with light turned off during data acquisition. A series of V_{TG} biases were applied from −1.0 to +1.0 V, after the I_D-V_{BG} curve was taken at V_{TG} = 0.0 V (black). The application of V_{TG} bias of −1.0 V makes the V_{Dirac} shift to positive potentials, and results in a significant hysteresis in the V_{Dirac} locations (by ∼0.8 V) between the two I_D-V_{BG} curves measured at V_{TG} = 0.0 V before (black) and after (pink) the application of the negative V_{TG} biases. This indicates that a negative V_{TG} can accelerate recovery of the self-organized TFSI layer on the IL/graphene interface. Interestingly, and different from the case of no light exposure (Figure 2d), the total V_{Dirac} shifts are about 1 V under the V_{TG} bias change from −1.0 to +1.0 V, which was comparable to that of a device with a freshly applied DEME-TFSI top-gate (Figure 2c). In particular, a similar linear $V_{Dirac}-V_{TG}$ curve (red) with a slope of ∼0.49, comparable to that of the GFET with pristine surface (black) can be seen in Figure 6b. All of these observations indicate that a newly formed self-organized TFSI layer after light illumination differs from the one before light illumination of stronger "pinning" effect, which prevents the electrostatic response to the applied V_{TG} biases. The formation of a new layer after light illumination may be attributed to the fact that pinned molecular ions in this layer were set free again or that the molecular activity of the ions was changed as a result of the electrochemical effect at the interface was reduced under light illumination. The newly formed self-organized TFSI layer can explain the large disagreement between the I_D-V_{BG} curves at V_{TG} = 0.0 V before and after V_{TG} = −1.0 V was applied (Figure 6c). Remarkably, applying the V_{TG} in an opposite sequence starting from V_{TG} = +1.0 V may prevent formation of the self-organized TFSI on the interface as illustrated in the overlapping I_D-V_{BG} curves at V_{TG} = 0.0 V before and after V_{TG} = +1.0 V was applied (Figure 6d).

CONCLUSIONS

In conclusion, double-gate GFETs with a PLZT back-gate of compatible gating efficiency to the IL top-gate were used to investigate molecular ions' behavior at the IL/graphene interface. It is found that the TFSI anion molecules are sensitive to the surface conditions of the graphene, and self-organize on graphene to cause GFET hole-doping. Moreover, a dynamic and reversible order-to-disorder transition of the TFSI anion layer was illustrated, when it was illuminated by ultraviolet−visible light. This work hence sheds lights on the microscopic origin of the electrochemical effect on the graphene surface and is important to a variety of electrochemical applications involving electrolyte/carbon interfaces.

ASSOCIATED CONTENT

Supporting Information

The Supporting Information is available free of charge on the ACS Publications website at DOI: 10.1021/acsami.7b10912.

Specific capacitance calculation and measurement, assessment of the gate efficiency ratio between the top-gate and back-gate, and the emission spectrum of the white light source used (PDF)

AUTHOR INFORMATION

Corresponding Authors

*E-mail: chunrui.ma@mail.xjtu.edu.cn.
*E-mail: jwu@ku.edu.

ORCID

Chunrui Ma: 0000-0002-7824-7930
Ming Liu: 0000-0002-4392-9659
Jun Li: 0000-0002-3689-8946
Scott K. Shaw: 0000-0003-3767-3236

Notes

The authors declare no competing financial interest.

ACKNOWLEDGMENTS

The authors acknowledge support in part by NASA Contract NNX13AD42A, ARO Contract W911NF-16-1-0029, and NSF Contract NSF-DMR-1337737 and NSF-DMR1508494. This research also was supported by the Natural Science Foundation of China 51390472, National "973" projects of China (2015CB654903), China postdoctoral science Foundation 2015M582649, NSFC-NGC 61631166004, and the Fundamental Research Funds for the Central Universities. S.K.S. acknowledges funding from NSF Award 1651381, ACS-PRF Award 55279-DNI5, and the Research Corporation for Science Advancement's Cottrell Scholar award funding.

DOI: 10.1021/acsami.7b10912
ACS Appl. Mater. Interfaces 2017, 9, 35437−35443

REFERENCES

(1) Veerasubramani, G. K.; Krishnamoorthy, K.; Pazhamalai, P.; Kim, S. J. Enhanced Electrochemical Performances of Graphene Based Solid-State Flexible Cable Type Supercapacitor Using Redox Mediated Polymer Gel Electrolyte. *Carbon* **2016**, *105*, 638−648.

(2) Shi, M.; Kou, S.; Yan, X. Engineering the Electrochemical Capacitive Properties of Graphene Sheets in Ionic-Liquid Electrolytes by Correct Selection of Anions. *ChemSusChem* **2014**, *7*, 3053−3062.

(3) Abalyaeva, V. V.; Baskakov, S. A.; Dremova, N. N. Composite Materials Based on Reduced Graphene Oxide and Polyaniline. Composition, Morphology, Electrochemical Properties. *Russ. J. Electrochem.* **2015**, *51*, 916−924.

(4) Jiang, D.-E. Graphene/Electrolyte Interface in Electrochemical Energy Storage: From Supercapacitors to Li-Ion Batteries. *Abstr. Pap.—Am. Chem. Soc.* **2012**, 228.

(5) Prakash, A.; Bahadur, D. The Role of Ionic Electrolytes on Capacitive Performance of ZnO-Reduced Graphene Oxide Nanohybrids with Thermally Tunable Morphologies. *ACS Appl. Mater. Interfaces* **2014**, *6*, 1394−1405.

(6) Rao, C. N. R.; Gopalakrishnan, K.; Maitra, U. Comparative Study of Potential Applications of Graphene, MoS_2, and Other Two-Dimensional Materials in Energy Devices, Sensors, and Related Areas. *ACS Appl. Mater. Interfaces* **2015**, *7*, 7809−7832.

(7) Miskovic, Z. L.; Sharma, P.; Goodman, F. O. Ionic Screening of Charged Impurities in Electrolytically Gated Graphene. *Phys. Rev. B: Condens. Matter Mater. Phys.* **2012**, *86*, 115437.

(8) Chen, F.; Xia, J.; Tao, N. Ionic Screening of Charged-Impurity Scattering in Graphene. *Nano Lett.* **2009**, *9*, 1621−1625.

(9) Zheng, W.; Mohammed, A.; Hines, L. G.; Xiao, D.; Martinez, O. J.; Bartsch, R. A.; Simon, S. L.; Russina, O.; Triolo, A.; Quitevis, E. L. Effect of Cation Symmetry on the Morphology and Physicochemical Properties of Imidazolium Ionic Liquids. *J. Phys. Chem. B* **2011**, *115*, 6572−6584.

(10) Akbulut, M.; Chen, N. H.; Maeda, N.; Israelachvili, J.; Grunewald, T.; Helm, C. A. Crystallization in Thin Liquid Films Induced by Shear. *J. Phys. Chem. B* **2005**, *109*, 12509−12514.

(11) Chu, M. Q.; Miller, M.; Dutta, P. Crowding and Anomalous Capacitance at an Electrode-Ionic Liquid Interface Observed Using Operando X-ray Scattering. *ACS Cent. Sci.* **2016**, *2*, 175−180.

(12) Atkin, R.; Borisenko, N.; Druschler, M.; Endres, F.; Hayes, R.; Huber, B.; Roling, B. Structure and Dynamics of the Interfacial Layer Between Ionic Liquids and Electrode Materials. *J. Mol. Liq.* **2014**, *192*, 44−54.

(13) Perkin, S.; Albrecht, T.; Klein, J. Layering and Shear Properties of an Ionic Liquid, 1-Ethyl-3-Methylimidazolium Ethylsulfate, Confined to Nano-Films between Mica Surfaces. *Phys. Chem. Chem. Phys.* **2010**, *12*, 1243−1247.

(14) Hettige, J. J.; Araque, J. C.; Margulis, C. J. Bicontinuity and Multiple Length Scale Ordering in Triphilic Hydrogen-Bonding Ionic Liquids. *J. Phys. Chem. B* **2014**, *118*, 12706−12716.

(15) Roy, D.; Maroncelli, M. Simulations of Solvation and Solvation Dynamics in an Idealized Ionic Liquid Model. *J. Phys. Chem. B* **2012**, *116*, 5951−5970.

(16) Kimura, Y.; Fukuda, M.; Suda, K.; Terazima, M. Excited State Intramolecular Proton Transfer Reaction of 4′-N,N-Diethylamino-3-hydroxyflavone and Solvation Dynamics in Room Temperature Ionic Liquids Studied by Optical Kerr Gate Fluorescence Measurement. *J. Phys. Chem. B* **2010**, *114*, 11847−11858.

(17) Goodwin, Z. A. H.; Kornyshev, A. A. Underscreening, Overscreening and Double-Layer Capacitance. *Electrochem. Commun.* **2017**, *82*, 129−133.

(18) Du, X. W.; Guo, H.; Jin, Y.; Jin, Q. H.; Zhao, J. L. Electrochemistry Investigation on the Graphene/Electrolyte Interface. *Electroanalysis* **2015**, *27*, 2760−2765.

(19) Cole, D. J.; Ang, P. K.; Loh, K. P. Ion Adsorption at the Graphene/Electrolyte Interface. *J. Phys. Chem. Lett.* **2011**, *2*, 1799−1803.

(20) Weiss, N. O.; Zhou, H.; Liao, L.; Liu, Y.; Jiang, S.; Huang, Y.; Duan, X. Graphene: an Emerging Electronic Material. *Adv. Mater.* **2012**, *24*, 5782−5825.

(21) Ma, C.; Lu, R.; Hu, G.; Han, J.; Liu, M.; Li, J.; Wu, J. Detecting Electric Dipoles Interaction at the Interface of Ferroelectric and Electrolyte Using Graphene Field Effect Transistors. *ACS Appl. Mater. Interfaces* **2017**, *9*, 4244−4252.

(22) Ma, C. R.; Ma, B. H.; Mi, S. B.; Liu, M.; Wu, J. Enhanced Dielectric Nonlinearity in Epitaxial $Pb_{0.92}La_{0.08}Zr_{0.52}Ti_{0.48}O_3$ Thin Films. *Appl. Phys. Lett.* **2014**, *104*, 162902.

(23) Brown, E.; Ma, C.; Acharya, J.; Ma, B.; Wu, J.; Li, J. Controlling Dielectric and Relaxor-Ferroelectric Properties for Energy Storage by Tuning $Pb_{0.92}La_{0.08}Zr_{0.52}Ti_{0.48}O_3$ film thickness. *ACS Appl. Mater. Interfaces* **2014**, *6*, 22417−22422.

(24) Xu, G. W.; Lu, R. T.; Liu, J. W.; Chiu, H. Y.; Hui, R. Q.; Wu, J. Z. Photodetection Based on Ionic Liquid Gated Plasmonic Ag Nanoparticle/Graphene Nanohybrid Field Effect Transistors. *Adv. Opt. Mater.* **2014**, *2*, 729−736.

(25) Ma, C.; Gong, Y.; Lu, R.; Brown, E.; Ma, B.; Li, J.; Wu, J. Detangling Extrinsic and Intrinsic Hysteresis for Detecting Dynamic Switch of Electric Dipoles Using Graphene Field-Effect Transistors on Ferroelectric Gates. *Nanoscale* **2015**, *7*, 18489−18497.

(26) Balasubramanian, K.; Sordan, R.; Burghard, M.; Kern, K. A Selective Electrochemical Approach to Carbon Nanotube Field-Effect Transistors. *Nano Lett.* **2004**, *4*, 827−830.

(27) Kruger, M.; Buitelaar, M. R.; Nussbaumer, T.; Schonenberger, C.; Forro, L. Electrochemical Carbon Nanotube Field-Effect Transistor. *Appl. Phys. Lett.* **2001**, *78*, 1291−1293.

(28) Ueno, K.; Shimotani, H.; Iwasa, Y.; Kawasaki, M. Electrostatic Charge Accumulation Versus Electrochemical Doping in $SrTiO_3$ Electric Double Layer Transistors. *Appl. Phys. Lett.* **2010**, *96*, 252107.

(29) Frackowiak, E. Carbon Materials for Supercapacitor Application. *Phys. Chem. Chem. Phys.* **2007**, *9*, 1774−1785.

(30) Sato, T.; Maruo, T.; Marukane, S.; Takagi, K. Ionic Liquids Containing Carbonate Solvent as Electrolytes for Lithium Ion Cells. *J. Power Sources* **2004**, *138*, 253−261.

(31) Xu, S. Y.; Xing, S. R.; Pei, S. S.; Ivanistsev, V.; Lynden-Bell, R.; Baldelli, S. Molecular Response of 1-Butyl-3-Methylimidazolium Dicyanamide Ionic Liquid at the Graphene Electrode Interface Investigated by Sum Frequency Generation Spectroscopy and Molecular Dynamics Simulations. *J. Phys. Chem. C* **2015**, *119*, 26009−26019.

(32) Parr, D. I.; Chrestenson, J.; Malik, M. K.; Molter, M.; Zibart, C.; Egan, B.; Haverhals, L. M. Structure and Dynamics at Ionic Liquid/Electrode Interfaces. *ECS Trans.* **2015**, *66*, 35−42.

(33) Liu, Q. F.; Gong, Y. P.; Wilt, J. S.; Sakidja, R.; Wu, J. Synchronous Growth of AB-Stacked Bilayer Graphene on Cu by Simply Controlling Hydrogen Pressure in CVD Process. *Carbon* **2015**, *93*, 199−206.

(34) Ye, J. T.; Inoue, S.; Kobayashi, K.; Kasahara, Y.; Yuan, H. T.; Shimotani, H.; Iwasa, Y. Liquid-Gated Interface Superconductivity on an Atomically Flat Film. *Nat. Mater.* **2010**, *9*, 125−128.

(35) Lu, R. T.; Liu, J. W.; Luo, H. F.; Chikan, V.; Wu, J. Z. Graphene/GaSe-Nanosheet Hybrid: Towards High Gain and Fast Photoresponse. *Sci. Rep.* **2016**, *6*, 19161.

(36) Liu, Q. F.; Gong, Y. P.; Wang, T.; Chan, W. L.; Wu, J. Metal-Catalyst-Free and Controllable Growth of High-Quality Monolayer and AB-Stacked Bilayer Graphene on Silicon Dioxide. *Carbon* **2016**, *96*, 203−211.

(37) Yoshimura, Y.; Takekiyo, T.; Imai, Y.; Abe, H. Pressure-Induced Spectral Changes of Room-Temperature Ionic Liquid, N,N-Diethyl-N-methyl-N-(2-methoxyethyl)ammonium Bis(trifluoromethylsulfonyl)-imide, [DEME][TFSI]. *J. Phys. Chem. C* **2012**, *116*, 2097−2101.

(38) Liu, Q. F.; Cook, B.; Gong, M. G.; Gong, Y. P.; Ewing, D.; Casper, M.; Stramel, A.; Wu, J. D. Printable Transfer-Free and Wafer-Size MoS_2/Graphene van der Waals Heterostructures for High-Performance Photodetection. *ACS Appl. Mater. Interfaces* **2017**, *9*, 12728−12733.

DOI: 10.1021/acsami.7b10912
ACS Appl. Mater. Interfaces 2017, 9, 35437−35443

(39) Anaredy, R. S.; Lucio, A. J.; Shaw, S. K. Adventitious Water Sorption in a Hydrophilic and a Hydrophobic Ionic Liquid: Analysis and Implications. *Acs Omega* **2016**, *1*, 407−416.
(40) Anaredy, R. S.; Shaw, S. K. Long-Range Ordering of Ionic Liquid Fluid Films. *Langmuir* **2016**, *32*, 5147−5154.

DOI: 10.1021/acsami.7b10912
ACS Appl. Mater. Interfaces 2017, 9, 35437−35443